Nb$_4$N$_3$: Polymorphism in crystalline niobium nitrides

E. C. Ethridge, S. C. Erwin, and W. E. Pickett

Complex Systems Theory Branch, Naval Research Laboratory, Washington, DC 20375
(Received 13 December 1995)

Local-density-based electronic structure methods are applied to γ-NbN (tetragonal Nb$_4$N$_3$) to compare it to the strong-coupling superconductor NbN (rocksalt structure) and to the recently proposed $Pm3m$ NbN phase, (NbO structure) which has a similar transition temperature. In certain respects γ-NbN is intermediate between the other phases, as might be expected, but overall the electronic spectrum more closely resembles rocksalt NbN. The N ion in γ-NbN is more highly charged (N^{-1}) than in the other two phases. [S0163-1829(96)03420-0]

The Nb-N phase diagram contains several compounds that can be regarded as resulting from ordering of vacancies on one or both sublattices of the rocksalt NbN structure. Substoichiometry is common on the N sublattice, and the samples with relatively high superconducting transition temperature T_c are rarely if ever stoichiometric compounds. Evidently small substoichiometry does not affect T_c much, but it was surprising when Treece *et al.*[1] reported recently that a related phase with 25% ordered vacancies on both sublattices has essentially the same value of T_c (16.4 K) as rocksalt NbN.

Rather little is understood about how substoichiometry and the ordering of vacancies affects the electronic structure and thereby the phase stability in the Nb-N system. Superconductivity in NbN is dependent upon the crystal structure and the extent to which the phase deviates from stoichiometry. For example, while stoichiometric Nb$_4$N$_4$ (cubic rocksalt), Nb$_3$N$_3$ (simple cubic), Nb$_4$N$_3$ (tetragonal), and Nb$_4$N$_5$ (tetragonal) exhibit superconductivity with T_c ranging from 8.0 to 16.4 K, Nb$_5$N$_6$ (hexagonal) does not exhibit superconductivity down to 1.77 K.[1,2] We have previously studied the structural and electronic properties of the proposed ordered vacancy phase using full potential electronic structure methods and concluded that the stoichiometric $Pm3m$ phase is improbable.[3] Independent calculations corroborate these findings.[4] Because of this, we have begun exploring related Nb-N phases.

In this paper we present the results of a study of an ordered vacancy structure in the Nb-N system with a superconducting T_c near 11.5 K, γ-NbN. Thin films having the γ-NbN structure were fabricated on MgO (100) using the vapor-deposition technique nearly two decades ago.[2] γ-NbN is a tetragonal distortion of the rocksalt structure with 25% ordered vacancies on the metalloid sublattice. The experimental lattice parameters used in the electronic structure calculations are $a_s = a = 4.382$ Å , $c_s = 2c = 8.632$ Å, and the internal parameter is $z_{\text{Nb}} = 0.5042c$.[5] The structure is shown in Fig. 1, with both the c/a ratio and the out-of-plane distortion of the fivefold coordinated Nb atom exaggerated for illustration. The primitive unit cell contains four Nb and three N atoms. The loss of cubic symmetry gives rise to two distinct Nb atom types (highlighted): Nb(1) is fourfold coordinated with N, while Nb(2) is fivefold coordinated with N. There are also two N atom types: N(1) is fourfold coordinated with Nb(2) and twofold coordinated with Nb(1), while N(2) is fourfold coordinated with Nb(1) and twofold coordi-

nated with Nb(2). Our findings are contrasted with two other superconducting phases of N̲bN̲: the rocksalt structure, which has the space group $Fm3m$ and will be denoted by Nb$_4$N$_4$, and the rocksalt structure with one-quarter of the Nb and N removed, which has the space group $Pm3m$ and will be denoted by Nb$_3$N$_3$. The tetragonally distorted rocksalt structure, γ-NbN, with one-quarter of the N removed, has the space group $I4/mmm$, and will be referred to as Nb$_4$N$_3$.

Using the full-potential, all-electron method of linear combination of atomic orbitals, density functional band-structure and total-energy calculations were carried out for Nb$_4$N$_3$. This approach, which is described elsewhere, parallels the previously reported electronic band calculations of
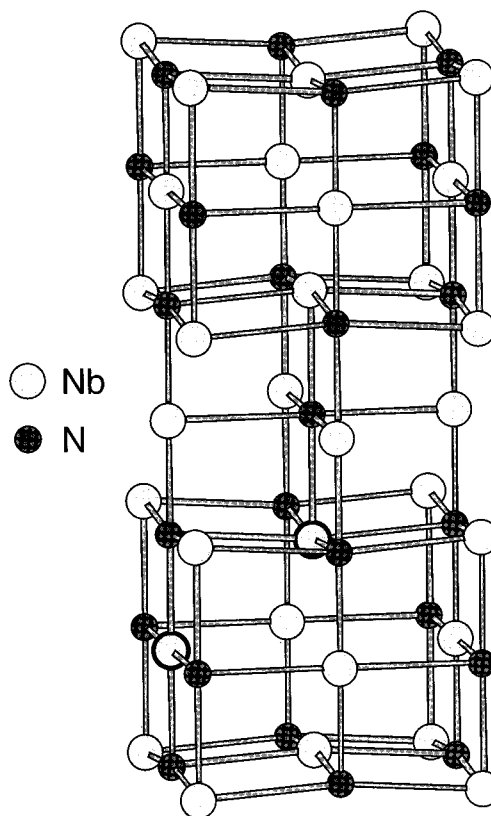

FIG. 1. Crystal structure of Nb$_4$N$_3$. Nb atoms occupy both fivefold and fourfold coordinated sites (heavy outlines). For illustration, exaggerated values were chosen for c/a and for the out-of-plane relaxation of the fivefold-coordinated Nb.
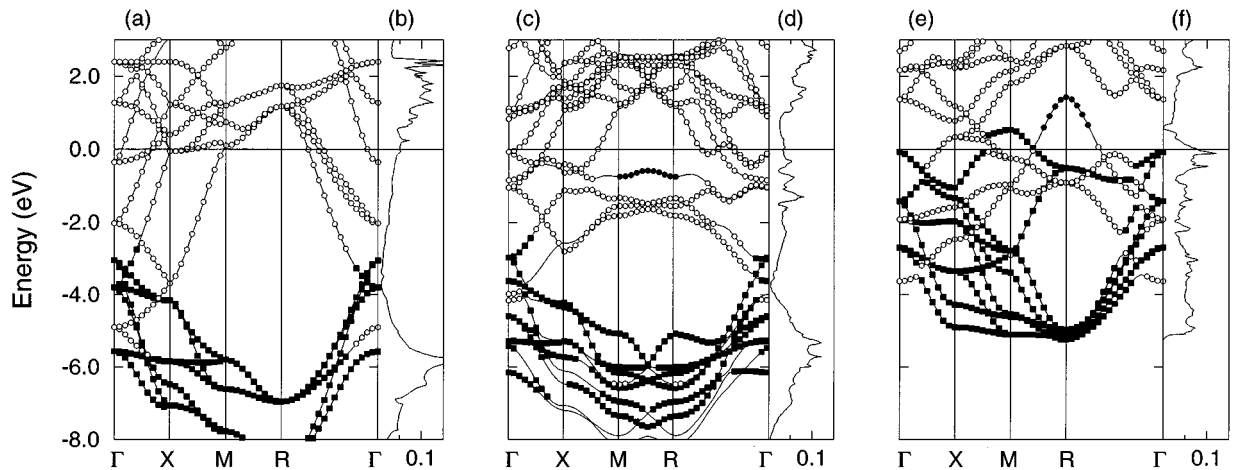
FIG. 2. Self-consistent electronic band structure and density of states (DOS) for (a),(b) Nb_4N_4 (c),(d) Nb_4N_3, and (e),(f) Nb_3N_3. The character of each band is indicated. Filled squares denote N p character, filled circles denote Nb p character, and open circles denote Nb d character. DOS is in states/eV $Å^3$. The Fermi level is the energy zero. Band structures are computed at the high-symmetry points of the primitive cell of the Nb_3N_3 structure.

Nb_4N_4 and Nb_3N_3.[3,6] The basis functions were expanded in a set of 17 Gaussian exponents contracted into seven s-type, five p-type, and four d-type functions for Nb, and 12 exponents contracted into four s-type and three p-type functions for N. The self-consistent band structure and total energies were computed using the Perdew-Zunger exchange-correlation potential[7] within a local-density approximation (LDA) and 15 special k points in the irreducible Brillouin zone. For the density-of-states (DOS) calculation, energies were calculated at 125 k points in the irreducible zone, interpolated to a denser grid using a Fourier spline method,[8] and integrated with the linear tetrahedron method.[9]

The band structure and DOS of each NbN phase we considered are shown in Fig. 2. To compare the three phases, the band-structure calculations are shown at the high-symmetry points in the primitive unit cell of the Nb_3N_3 structure. Mulliken population analysis was used to determine the orbital character of each band.[10] The dominant character of each band is indicated.

The DOS for the Nb_4N_4 structure, shown in Fig. 2(b), is concentrated in two broad peaks. The low-energy peak, between -8.6 and -3.5 eV (the zero of energy is taken at the Fermi energy E_F), is comprised mostly of N p states with

small admixture of Nb d states, as indicated in the corresponding band structure. The other broad peak, lying at and above E_F, has Nb d character and is responsible for the $N(E_F)$ of 0.0499 states/eV $Å^3$.

Comparing to Nb_4N_4, the removal of one-fourth of the N atoms in Nb_4N_3 has a pronounced effect on the Nb states. In Fig. 2(d), a low-energy peak similar to that observed in the DOS for Nb_4N_4 is present but a redistribution of the spectral weight of the Nb d states results in a more diffuse DOS at higher energies. $N(E_F)$ is 0.0318 states/eV $Å^3$, lower than in Nb_4N_4. In addition, one of the bands [Fig. 2(c)] below E_F has Nb p character between the symmetry points M and R. Mulliken population analysis shows this to originate from fourfold coordinated Nb(1), and that this is the only region for which Nb p states are present within the Nb d complex. The bands derived from the remaining $2p$ states of the N atoms lie in the same energy region as they do in Nb_4N_4.
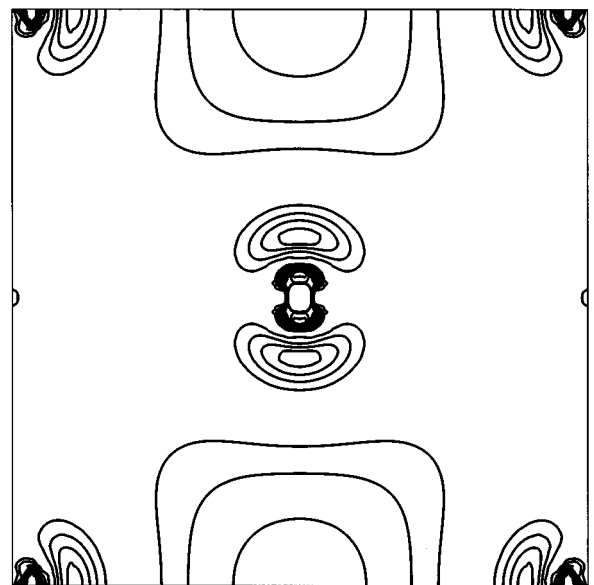
TABLE I. Decomposed valence charge distribution of Nb and N in the Nb_4N_4, Nb_4N_3, and Nb_3N_3 phases. For the Nb_4N_3 phase, columns 1 and 2 correspond to atom types 1 and 2 as described in the text. All calculations use the basis sets described in the text.

Orbital	Nb_4N_4	Nb_4N_3		Nb_3N_3
N s	1.98	1.88	1.91	1.76
N p	3.83	4.10	4.16	3.84
Net N charge	-0.81	-0.98	-1.07	-0.60
Nb s	0.37	0.41	0.42	0.47
Nb p	0.06	0.09	0.06	0.33
Nb d	3.76	3.82	3.69	3.60
Net Nb charge	$+0.81$	$+0.68$	$+0.83$	$+0.60$

FIG. 3. Contour plot of the self-consistent charge density for Nb_4N_3 in a (100) plane. Centered in the figure is a Nb(1) atom with its p orbital directed toward N vacancy sites (above and below).

For the Nb_3N_3 band structure, shown in Fig. 2(e), a significant upward shift and redistribution of the N p states is apparent. The manifold of N p bands is raised by nearly 2 eV and the Fermi level falls in an energy region where both N p and Nb d bands are occupied. Above E_F, a band with Nb p character is centered at the R point. The enhancement in the DOS at the Fermi level [$N(E_F) = 0.0788$ states/eV Å^3] results primarily from the Nb d states. The electronic structure of Nb_3N_3 has been discussed in detail elsewhere.[3]

According to Mulliken population analysis, Nb_4N_3 is more ionic than Nb_4N_4 and Nb_3N_3 with respect to the net N charge. In Table I, the effective charge on each atom is separated by orbital type. The total charge transfered from Nb to N is 0.81 and 0.60 for Nb_4N_4 and Nb_3N_3, respectively. In Nb_4N_3, the charge transfer is anisotropic. N(1) has an excess charge of 0.98 while N(2) has an excess charge of 1.07, and the net charges on the two Nb sites differ by 0.15 electron (Table I). In both cases, the excess charge appears in the N p states. The total effective charge on the Nb p orbitals is comparable in Nb_4N_3, but angular decomposition shows the p orbitals on Nb(1), which are directed toward vacancy sites retain more charge. They give rise to the occupied band with Nb p character in Fig. 3(c), which occurs near -0.75 eV between the high-symmetry points M and R. A contour plot of the self-consistent charge density in a (100) plane computed for this band between M and R (shown in Fig. 4) exemplifies this behavior.

We have also carried out total-energy calculations to examine the equilibrium crystal structure of Nb_4N_3. The results of our total-energy calculations are shown in Fig. 4. The cell volume V and c/a ratio were varied independently over a range of values within $\pm 8\%$ of experiment (the single internal parameter was scaled proportionally, but was not optimized). At each volume, the optimal c/a and corresponding $E(V)$ were determined by fitting the total energy to a third-order polynomial in c/a; the resulting values of $E(V)$ were then fit to a Birch[11] equation of state. At equilibrium, we obtain the theoretical lattice parameters $a = 4.316$ Å and $c = 4.358$ Å, respectively, 1.5% smaller and 1.0% larger than experiment. The theoretical c/a ratio is 1.010, compared to the experimental value of 0.985. While these discrepancies are somewhat larger than one expects from LDA, they suggest that the x-ray diffraction results are generally consistent with our theoretical results. The theoretical bulk
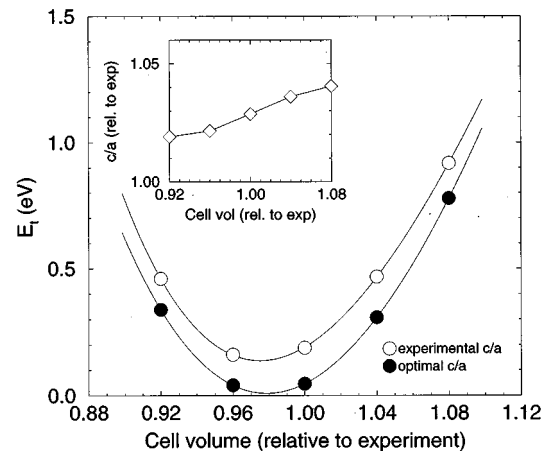

FIG. 4. Total energy calculations for the equilibrium cell volume and c/a ratio of Nb_4N_3. The open circles represent total-energy calculations that hold the c/a ratio fixed at the experimental value. The filled circles represent total-energy calculations in which the c/a ratio has been optimized. The inset shows the volume and optimal c/a ratio at which the filled circles are computed. The lines represent fits to the Birch equation.

modulus is 3.29 Mbar, slightly lower than our earlier results for the $B1$ and NbO phases of NbN (3.57 and 2.97 Mbar, respectively).

By comparing the three superconducting phases of NbN, we have been able to systematically study the effects of ordered vacancies on the N sublattice or on both the Nb and N sublattices and interpret the structural and spectral changes. While the band structures and DOS in Fig. 2 reflect the similarities between Nb_4N_4 and Nb_4N_3, they also make apparent the origin of the dispersive band in Nb_3N_3 with Nb d character below E_F and Nb p character above E_F. In Nb_4N_3, Nb p states first appear slightly below E_F and according to Mulliken population analysis, are a manifestition of the reduced N coordination of the Nb(1) atoms. In Nb_3N_3, the removal of 25% of the Nb atoms results in all Nb atoms being equivalent [Nb(1) type] and a lowering of E_F.

[1] R.E. Treece, J.S. Horwitz, and D.B. Chrisey, in *Polycrystalline Thin Films: Structure, Texture, Properties and Applications*, edited by K. Barmak *et al.,* MRS Symposia Proceedings No. 343 (Materials Research Society, Pittsburgh, 1994), p. 747; R.E. Treece *et al.*, Appl. Phys. Lett. **65**, 2860 (1994); R.E. Treece, J.S. Horwitz, D.B. Chrisey, and E.P. Donovan, Chem. Mat. **6**, 2205 (1994); R.E. Treece *et al.*, Phys. Rev. B **51**, 9356 (1995).

[2] G. Oya and Y. Onodera, J. Appl. Phys. **45**, 1389 (1974).

[3] E.C. Ethridge, S.C. Erwin, and W.E. Pickett, Phys. Rev. B **52**, R8589 (1995).

[4] S. Öğüt and K.M. Rabe, Phys. Rev. B **52**, R8585 (1995).

[5] P. Villars and L.D. Calvert, *Pearson's Handbook of Crystallographic Data for Intermetallic Phases* (American Society of Metals, Metals Park, OH, 1991).

[6] S.C. Erwin, M.R. Pederson, and W.E. Pickett, Phys. Rev. B **41**, 10 437 (1990).

[7] J.P. Perdew and A. Zunger, Phys. Rev. B **23**, 5048 (1981).

[8] W.E. Pickett, H. Krakauer, and P.B. Allen, Phys. Rev. B **38**, 2721 (1988).

[9] G. Lehmann and M. Taut, Phys. Status Solidi B **54**, 469 (1972).

[10] R.S. Mulliken, J. Chem. Phys. **23**, 1833 (1955).

[11] F. Birch, J. Geophys. Res. **83**, 1257 (1978).